



Delft University of Technology

Aeroservoelastic flight testing platform development for system identification

Jurisson, A.; De Breuker, R.; de Visser, C.C.; Eussen, Bart; Timmermans, H

DOI

[10.2514/6.2022-2169](https://doi.org/10.2514/6.2022-2169)

Publication date

2022

Document Version

Final published version

Published in

AIAA SCITECH 2022 Forum

Citation (APA)

Jurisson, A., De Breuker, R., de Visser, C. C., Eussen, B., & Timmermans, H. (2022). Aeroservoelastic flight testing platform development for system identification. In *AIAA SCITECH 2022 Forum Article AIAA 2022-2169* (AIAA Science and Technology Forum and Exposition, AIAA SciTech Forum 2022). <https://doi.org/10.2514/6.2022-2169>

Important note

To cite this publication, please use the final published version (if applicable).
Please check the document version above.

Copyright

Other than for strictly personal use, it is not permitted to download, forward or distribute the text or part of it, without the consent of the author(s) and/or copyright holder(s), unless the work is under an open content license such as Creative Commons.

Takedown policy

Please contact us and provide details if you believe this document breaches copyrights.
We will remove access to the work immediately and investigate your claim.



Aeroservoelastic flight testing platform development for system identification

A. Jurisson*, R. de Breuker.[†], and C.C. de Visser.[‡]
Delft University of Technology, 2629 HS, Delft, The Netherlands

B. Eussen.[§] and H. Timmermans.[¶]
Netherlands Aerospace Centre, 1059 CM, Amsterdam, The Netherlands

Netherlands Aerospace Centre (NLR) and Delft University of Technology (TUD) have obtained an unmanned aerial vehicle to serve as a test platform for future aeroservoelastic flight testing. The purpose of this testbed is to collect data about flexible aircraft flight dynamic responses and loads on the aircraft at unsteady airflow conditions for flexible aircraft system identification. An overview of the 1:3 scaled Diana 2 glider is presented together with numerous tests that were conducted to characterise the test platform. Moment of inertia of the aircraft was determined using a pendulum and rotational swing setup, control surface dynamics were identified from sine sweeps and the structural modes and frequencies were obtained from a ground vibration test. Finally, a low cost and modular data acquisition system was built to collect all the sensor measurements. This data acquisition system is presented together with an overview of its performance.

I. Introduction

The pursuit for increased performance and efficiency is pushing the aircraft design towards wings with higher aspect ratios while also using lighter materials. The longer wingspan and lower structural stiffness in turn often leads to a closer interaction between the aircraft rigid-body responses and the aeroelastic effects due to the reduction in structural eigenfrequencies. Having an accurate understanding of this interaction is important to ensure the safety of the vehicle but also to develop high-fidelity flight simulators for pilot training, to design control laws in order to improve the aircraft performance and to monitor the resulting loads that are being exerted on the aircraft [1]. During the aircraft design process numerical models are created to simulate the aircraft response to manoeuvres in various flight conditions in order to determine the critical design loads. This process is combined with system identification methods in order to validate or update the model coefficients using wind tunnel and flight test measurements. When applying system identification to aircraft flight dynamics, the traditional approach is to analyse the flight test measurements by considering the rigid-body and structural dynamics as fully decoupled. However, this can lead to inaccurate results in the case of flexible aircraft where the decoupling assumption is suddenly violated. Therefore, it is necessary to develop system identification methods that could also accurately capture and model the responses of flexible aircraft. In order to develop and evaluate different system identification approaches for flexible aircraft, flight test data is needed. However, such experimental data from aeroelastic test flights is scarce and rarely publicly shared [2]. For this reason, it was required to obtain a test platform which exhibits a close coupling between the flexible aircraft structure and the rigid-body response.

Here an overview is given of the scaled Diana 2 glider model and the instrumentation suite that was developed and integrated in order to measure the responses of the aircraft and its structure. Furthermore, various tests were conducted in order to determine the aircraft characteristics, such as the moment of inertias, control surface dynamics and the structural eigenmodes. An overview of these tests is also presented.

*Ph.D. Student, Faculty of Aerospace Engineering, Aerospace Structures and Computational Mechanics Division, A.Jurisson@tudelft.nl, 2629 HS Delft, The Netherlands.

[†]Associate Professor, Faculty of Aerospace Engineering, Aerospace Structures and Computational Mechanics Division, R.DeBreuker@tudelft.nl, 2629 HS Delft, The Netherlands.

[‡]Assistant Professor, Faculty of Aerospace Engineering, Control and Simulation Division, c.c.devisser@tudelft.nl, 2629 HS Delft, The Netherlands

[§]Senior Researcher, Flight Physics and Loads Department, Bart.Eussen@nlr.nl, 1059 CM, Amsterdam, The Netherlands.

[¶]Researcher, Flight Physics and Loads Department, Huub.Timmermans@nlr.nl, 1059 CM, Amsterdam, The Netherlands.

II. Aeroservoelastic test platform

As the main goal of the project is to develop a methodology for identifying flight dynamics and loads models for flexible aircraft in unsteady airflow conditions, also the aircraft used for testing needs to be flexible and able to fly in the unsteady airflow region. Furthermore, the test aircraft needs to be very accessible in order to quickly iterate between different sensor configurations and flight test setups. Based on these requirements a scaled glider model was chosen as the test platform for this project. Gliders have very high aspect ratios which makes them aerodynamically efficient but also often results in increased flexibility. This potential in increased efficiency is also pushing the commercial aircraft development towards higher aspect ratios which makes a glider aircraft a good test aircraft to represent future commercial aircraft. In addition to flexibility, a benefit of operating a scaled glider model is that the rules and regulations for flying drones are less strict compared to flying (test) aircraft. This allows to change the sensor configuration on board the test aircraft without the need for certification. However, the downside can be the lack of free space for housing the extra sensors as the physical dimensions of the aircraft are much smaller and the need to pilot the aircraft remotely. Moreover, many scaled model wings are built with foam cores which can make placing the sensors even more difficult. For this reason, a model with hollow wings had to be acquired.

The obtained unmanned aerial vehicle is a 1:3 scaled model of the Diana 2 glider manufactured by Baudismodel[3]. This scaled glider model has a wing span of 5 m and a high aspect ratio of 24.3. It is a composite aircraft manufactured using both carbon and glass fibre sheets. An overview of the technical data is presented in Table 1 and an image of the model is presented in Fig. 1.

Table 1 Diana 2 model technical data.

Property	Symbol	Value
Aspect ratio	Λ	24.3
Wingspan	b	5.0 m
Wing area	S	1.03 m^2
Mean aerodynamic chord (MAC)	\bar{c}	0.206 m
Weight	m	11.51 kg



Fig. 1 Diana 2 1:3 scaled glider.

The model has 3 ailerons on both wings which can also be configured as flaperons and/or spoilerons, 2 control surfaces for elevator and 1 rudder. There is also a Front Electric Self-launch/Self-sustainer (FES) propulsion system with folding propellers which allows for take-offs without a winch and greatly increases the endurance while simplifying the operations. Table 2 presents an overview of the servos used for the control surfaces, landing gear and the electric motor.

Table 2 Diana 2 servos and FES.

Type	Servo	Voltage range	Torque range
Ailerons	KST X10	6.0-8.4 V	7.5-10.8 kg.cm
Elevators	MKS HV6110	6.0-8.4 V	2.6-3.4 kg.cm
Rudder	MKS HV6130H	6.0-8.4 V	6.0-8.1 kg.cm
Landing gear	HS 5585MH	6.0-7.4	14.0-17.0 kg.cm
FES	Hacker A40-8L V4 14-Poles	22.2 V	-

As the Diana 2 scaled model was not designed and built in house, it was necessary to determine various properties of the glider in an experimental manner.

A. Moment of inertia determination

Knowing the moment of inertia of an aircraft is an important part of understanding the forces and moments that are acting on the aircraft. The moment of inertia of the Diana 2 was estimated using an experimental swing setup. In such a setup, the aircraft is suspended with cables and made to oscillate around the axis of interest with a small amplitude. The oscillation period is then measured and averaged over multiple oscillations to find the moment of inertia [4].

First, the aircraft pitch moment of inertia I_{yy} was determined. The test setup is presented in Fig. 2 where the aircraft is suspended from two points with four cables and oscillated in a back and forth motion. The oscillations were then recorded using an inertial measurement unit (IMU) attached to the aircraft. Tests were conducted at two different swing lengths and repeated twice. The oscillation frequencies for each test were found by determining the spectral density of the responses which are presented in Fig. 3.



Fig. 2 Pitch moment of inertia setup.

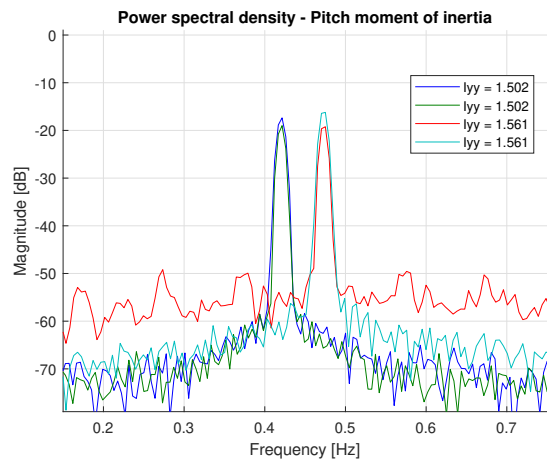


Fig. 3 Pitch moment of inertia response frequencies.

With the measured oscillation period it is then possible to estimate the pitch moment of inertia using Eq. 1 [4, 5].

$$I_{yy} = mgl \left(\frac{\tau}{2\pi} \right)^2 - ml^2 \quad (1)$$

where m is the mass of the model, l is the distance from the axis of rotation to the center of gravity, g is the gravitational acceleration and τ is the measured oscillation period.

Next, the yaw and roll moments of inertia were determined. Figure 4 and Fig. 5 present the setup for these experiments. Here the aircraft is suspended from two points with two cables and then oscillated in a rotational motion. Again the measured oscillation frequencies are presented in Fig. 6 and Fig.7.



Fig. 4 Yaw moment of inertia setup.



Fig. 5 Roll moment of inertia setup.

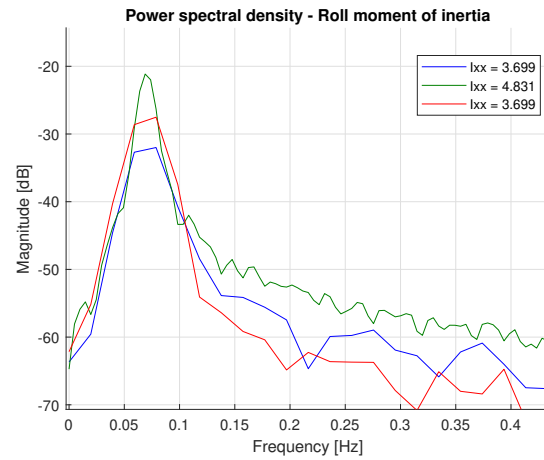
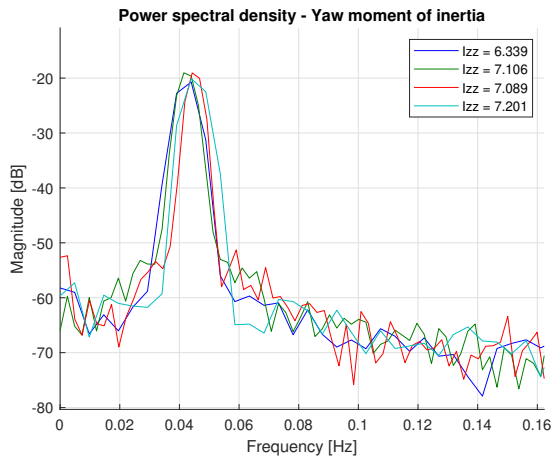


Fig. 6 Yaw moment of inertia response frequencies. Fig. 7 Roll moment of inertia response frequencies.

With the measured oscillation period it is then possible to estimate the yaw and roll moment of inertia using Eq. 2 for the rotational pendulums [4, 5]

$$I = \frac{mgd^2}{4l} \left(\frac{\tau}{2\pi} \right)^2 \quad (2)$$

where m is the mass of the model, d is the distance between the two suspension points, l is the distance from the suspension point to the center of gravity, g is the gravitational acceleration and τ is the measured oscillation period.

However, as can be seen from Fig. 5, the aircraft body axis in the roll test is at an angle to the axis of rotation.

Therefore, a correction transformation was applied to the measured moment of inertia to rotate it to the aircraft body axis. The angle between the aircraft body axis and the measured rotation axis was measured to be -5 deg. The applied transformation is presented in Eq. 3. As can be seen, this transformation also gives a product of inertia I_{xz} component.

$$\begin{bmatrix} 0 & 0 & I_{xz} \\ 0 & 0 & 0 \\ I_{xz} & 0 & I_{zz} \end{bmatrix} = \begin{bmatrix} \cos \theta & 0 & \sin \theta \\ 0 & 1 & 0 \\ -\sin \theta & 0 & \cos \theta \end{bmatrix} \begin{bmatrix} 0 & 0 & 0 \\ 0 & 0 & 0 \\ 0 & 0 & I'_{zz} \end{bmatrix} \begin{bmatrix} \cos \theta & 0 & \sin \theta \\ 0 & 1 & 0 \\ -\sin \theta & 0 & \cos \theta \end{bmatrix}^T \quad (3)$$

In Table 3, the averaged oscillation periods and moments of inertia are presented. The weight of the aircraft during the testing was measured 8.65 kg as it was conducted without installing batteries.

Table 3 Diana 2 model moment of inertia estimates.

	τ_{avg}	l	d	Moment of inertia
I_{xx}	13.61 s	0.966 m	0.203 m	4.2461 kgm^2
I_{yy}	2.37 s	1.262 m	-	1.5311 kgm^2
I_{zz}	23.05 s	2.1 m	0.219 m	6.8810 kgm^2
I_{xz}				-0.6020 kgm^2

B. Structural model and ground vibration test

In order to obtain a structural model of the Diana 2 for aeroelastic analysis, first an initial NASTRAN model was created based on the outer geometry supplied by the manufacturer. However, no information was obtained concerning the structural properties so a simplified beam model was created to provide a first estimation of the sensor placement for the ground vibration testing (GVT). The outer geometry and the NASTRAN model are presented in Fig. 8.

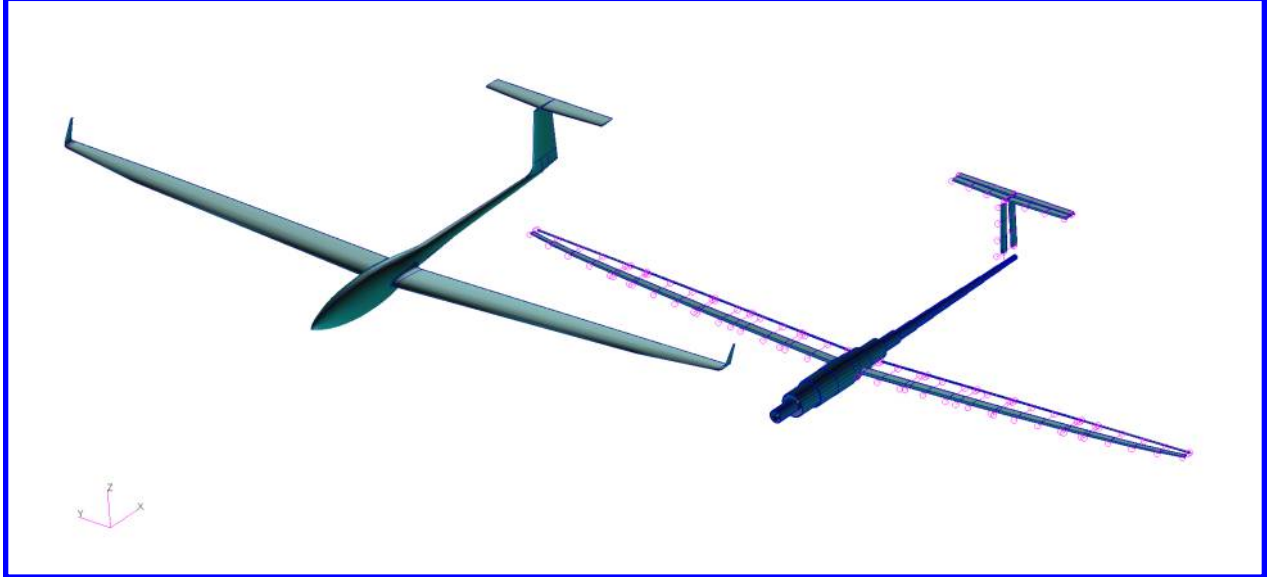


Fig. 8 Diana 2 model outline and NASTRAN model.

Next, a ground vibration test was conducted using the sensor configuration presented in Fig. 10. For the test, the aircraft was suspended in the air with elastic bands and excited with an impulse hammer at various locations. The aircraft structural response was then recorded using in total 47 acceleration measurement. This test setup can be seen in Fig. 9.

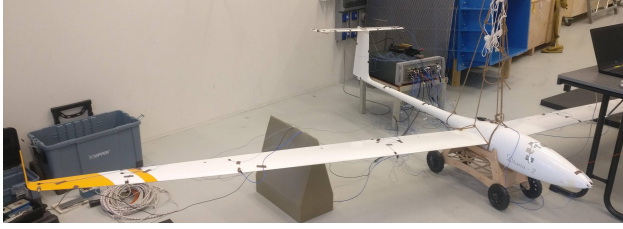


Fig. 9 Ground vibration testing setup.

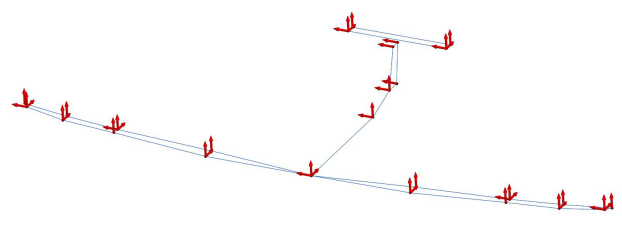


Fig. 10 Accelerometer locations during GVT.

From the GVT measurements, structural dynamic characteristics in terms of eigenfrequencies and eigenmodes, were first identified and then used to update the NASTRAN model. The results, in terms of Modal Assurance Criterion (MAC) and difference in eigenfrequency, are shown in Table 4. In general, there is a high correlation in terms of eigenmodes and eigenfrequency. The larger differences in the MAC values are mainly due to some of the GVT test points not having measurements for all degrees of freedom. Examples of the fitted NASTRAN model modeshapes are presented in Fig. 11 to Fig. 16.

Table 4 Correlation between fitted FEM model and GVT results.

Eigenmode	Nastran Eigenfreq [Hz]	GVT Eigenfreq [Hz]	Diff. [%]	MAC [%]
1st wing bending	7.546	7.550	-0.05	98.0
Vertical tail bending	10.06	9.946	1.12	90.1
Vertical tail torsion	15.61	14.19	10.04	79.3
2nd asym wing bending	16.98	17.31	-1.91	97.0
1st inplane wing bending	20.54	20.13	2.05	67.7
Fuselage side bending	22.55	21.25	6.12	65.9
Fuselage bending and 2nd wing bending	23.68	23.71	-0.13	63.6
2nd wing bending and fuselage bending	26.89	26.11	3.00	89.3
Fuselage side bending/ 3rd asym wing bending	41.34	39.84	3.77	42.0
3rd asym wing bending/ fuselage side bending	45.62	44.98	1.42	76.7
Horizontal tail bending	48.19	46.99	2.56	96.1
Horizontal tail bending and wing torsion	56.41	53.25	5.94	84.0
Wing torsion	61.81	63.20	-2.19	47.3

In order to increase the interaction between the aircraft rigid body motion and the structural dynamics, making modifications to the aircraft will be explored in the future. An example would be to add extra mass to the wingtips to lower the structural frequencies.

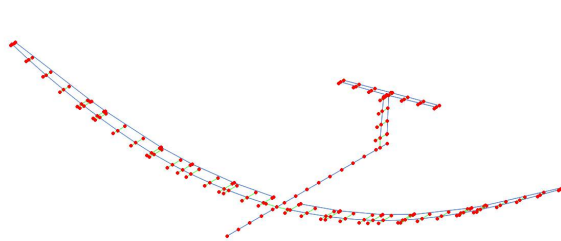


Fig. 11 First wing bending mode.

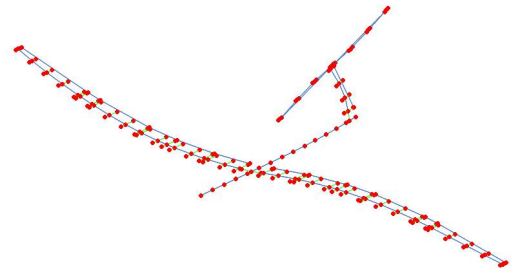


Fig. 12 Vertical tail bending mode.

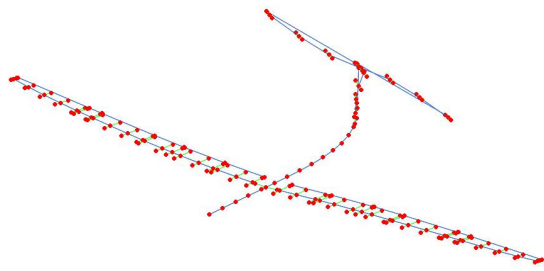


Fig. 13 Vertical tail torsion mode.

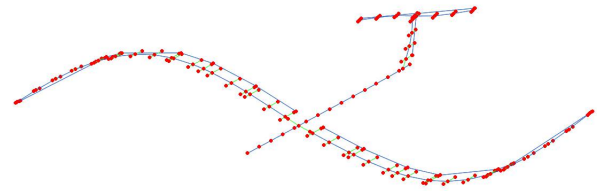


Fig. 14 Second asymmetric wing bending mode.

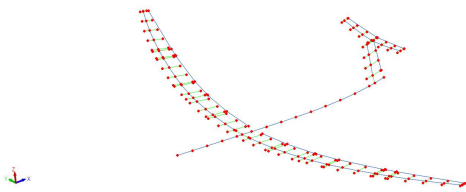


Fig. 15 First inplane wing bending mode.

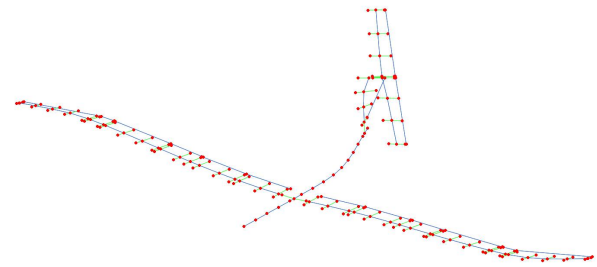


Fig. 16 Fuselage side bending mode.

C. Control surface dynamics testing

In order to model the dynamics of each control surface, first a reference command consisting of a sine sweep and step references was given to each surface up to a frequency of 10Hz at an amplitude of 25 percent of each control surface full range.

$$\delta_{ref} = A \sin(\omega t), \omega \in [0.1 \ 10] \text{ Hz} \quad (4)$$

The control surface responses were then measured using magnetic rotary encoders attached at the servo axis. In Fig. 17 the reference signal together with the right outer aileron response is presented as an example. In Fig. 18 the coherence signals between the reference commands and the control surface responses are presented. As can be seen, the input and output signals show good coherence and linear behaviour over the tested frequency range.

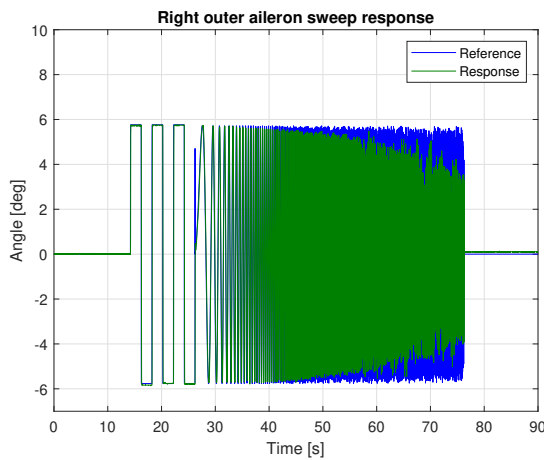


Fig. 17 Control surface reference signal and right outer aileron response.

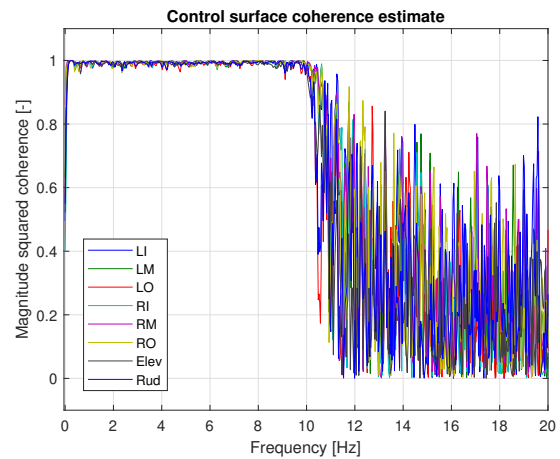


Fig. 18 Control surface response coherence.

Next, the reference and response angle signals were used to fit a second order transfer function as presented in Eq. 5. The parameters that were identified are presented in Table 5 together with the corresponding Bode plot in Fig. 19.

$$G(s) = \frac{\omega^2}{s^2 + 2\zeta\omega s + \omega^2} \quad (5)$$

Table 5 Identified actuator dynamics parameters.

Control surface	ω [rad/s]	ζ [-]	Fit [%]
Aileron Right Outer	53.55	0.63	89.11
Aileron Left Outer	52.55	0.65	88.45
Aileron Right Middle	53.24	0.71	90.83
Aileron Left Middle	50.91	0.69	88.34
Aileron Right Inner	50.91	0.64	85.94
Aileron Left Inner	51.43	0.73	90.14
Elevator	53.75	0.99	89.10
Rudder	43.01	0.88	88.95

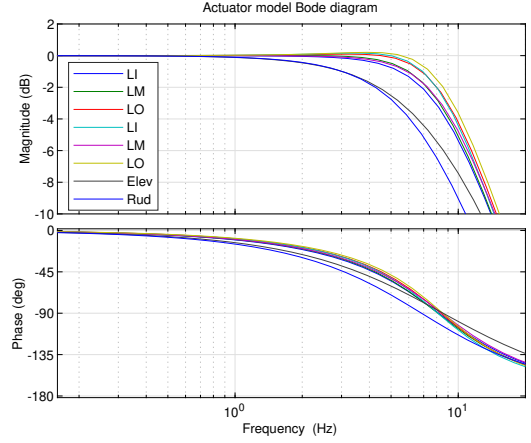


Fig. 19 Identified actuator model Bode plots.

In order to determine the mapping between the reference angle command and the corresponding output measurement, the control surfaces were moved slowly up and down while covering the entire range of motion. When evaluating these results it was noticed that there was a difference in the measured angle when the control surface was rising or being lowered. An example of this can be seen in Fig. 20 where the left middle aileron reference and response angles are normalized to -1 to 1 range and the top half is presented. These differences are likely due to freeplay between the servo gears and the linkage.

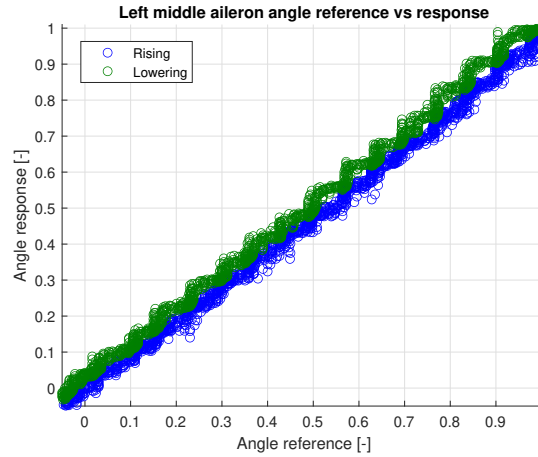


Fig. 20 Control surface freeplay - left middle aileron.

III. Instrumentation

To be able to capture the dynamic responses of the aircraft and its structure during flight together with the loads acting on the structure, a data acquisition system (DAQ) is needed. However, instrumenting the scaled Diana 2 glider posed several challenges. The space available inside the aircraft fuselage, wings, and tail is constrained. Furthermore, the extra weight that can be added to the aircraft and the electrical power available for the sensors is limited. To capture the response of the aircraft structure, many sensors across the entire aircraft are needed, so also a cost effective solution is preferred. Because of these requirements, a custom data acquisition system was developed for the scaled glider. An overview of the sensors together with the data acquisition system is presented in this section.

A. Autopilot

Having an autopilot on board the scaled glider is desirable firstly due to safety. In the case where the signal between the pilot and the glider is lost, the autopilot can take over the command and safely return the glider to base or loiter until the signal can be restored. In addition, an autopilot allows to measure the accelerations, rotations and atmospheric pressure at the center of gravity and log the commands given by the pilot. Furthermore, an autopilot is necessary to perform predefined excitations on the control surfaces such as multisines, sweeps etc. which would not be possible with manual control. Widely used and popular Pixhawk 4 autopilot hardware was selected for the Diana 2 which supports both the Ardupilot and PX4 open source autopilot software.

B. Data acquisition system

The data acquisition system consists of a Raspberry Pi 4 single board computer running on Linux operating system connected to multiple Teensy 4.0 development boards. An overview of the DAQ system is presented in Fig. 21. Here it can be seen, that the Teensy 4.0 boards are used to communicate with the individual sensors and collect the signals which are then collected centrally with the Raspberry Pi where the results are stored on a SD card.

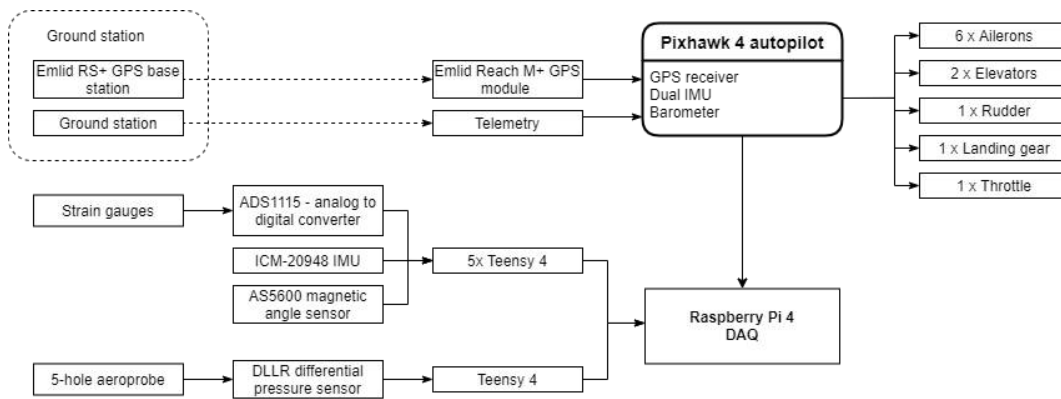


Fig. 21 Diana 2 DAQ system overview.

The Raspberry Pi is running Robot Operating System (ROS) to communicate with all the components. The *MAVROS* module allows to connect the Raspberry Pi to the Pixhawk 4 and retrieve all the sensor data and other parameters of interest from the autopilot while *rosserial* module allows to communicate with the Teensy 4.0-s to collect all the connected sensor measurements. ROS also synchronises the time signals between all the modules which allows to very accurately determine when each sample was collected. This modular design makes it easy to adapt or extend to different sensor configurations.

C. Aerodynamic angles

Important airflow parameters that need to be measured are the true airspeed, angle of attack and angle of sideslip. These measurements form the basis for the aircraft aerodynamic modelling. For this a 5-hole probe by Aeroprobe Corporation is used which is connected to three differential pressure sensors. The cleanest/ most uninterrupted measurement can be acquired when the probe is placed in the nose of the aircraft as the airflow there is not influenced by the fuselage or wings. However, due to the placement of the electric engine in the nose, a L-shaped probe placed to the side of the propeller was used instead as can be seen in Fig.22.



Fig. 22 Aeroprobe installation location.

To measure the pressure difference between the ports in the aeroprobe, the 18bit DLLR differential pressure sensors by Amphenol are used which have a maximum operating pressure of 10 inch H₂O (2488.4 Pa). In Fig 23 and Fig. 24 pressure difference measurement examples are presented for the angle of attack (AoA) and sideslip ports during step inputs for the elevator and pulses for the rudder.

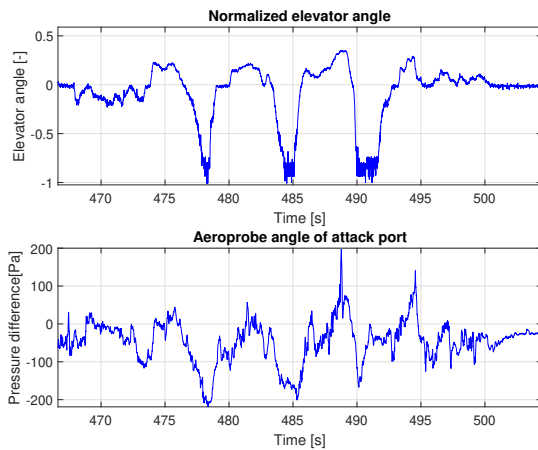


Fig. 23 AoA pressure difference measurement.

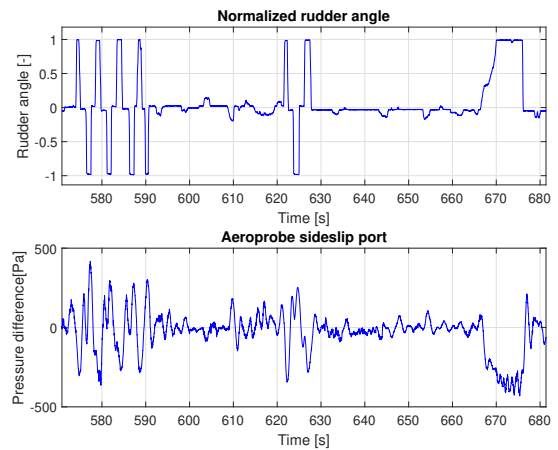


Fig. 24 Sideslip pressure difference measurement.

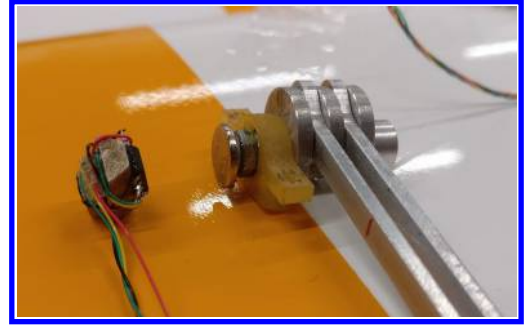
However, before the measured pressure differences can be converted to their corresponding angle of attack or angle of sideslip, a wind tunnel calibration of the aeroprobe and the sensors is needed.

D. Control surface angle

Measuring the control surface deflections is achieved using the AS5600 magnetic rotary encoders placed adjacent to the rotation axis of the servos with a diametrical magnet connected to the servo. The sensor has a 12bit resolution which allows to measure angle changes as small as 0.09 degrees without interfering with the servo. The sensor and the magnet attached to the control surface linkage before installation inside the wing are presented in Fig. 25. All control surface positions were measured together with the pulse-width modulation (PWM) command signals sent by the autopilot/receiver to establish a relation between them and determine the maximum range for each control surface. In Table 6 an overview of the range for each control surface is presented.

Table 6 Diana 2 control surface ranges.

Control surface	Range [deg]
Aileron outer	± 23
Aileron middle	± 20
Aileron inner	± 30
Elevator	± 20
Rudder	± 30

**Fig. 25 Magnetic rotary encoder (left) and magnet on the axis of the control surface linkage (right).**

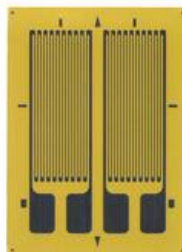
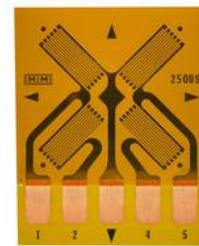
E. Aircraft position

The aircraft position is determined using a GPS antenna placed on the top of the fuselage and a receiver. In addition, a ground base station with a fixed/known location is used to improve the positioning accuracy using a technique called Real Time Kinematics (RTK). Here the base station estimates the errors/biases in the measurement area and passes the correction information to the drone over a telemetry link. The system selected for the Diana 2 includes the Reach M+ receiver and Reach RS+ base station by Emlid which allow to measure the aircraft position at a rate up to 14Hz.

F. Wing shape and loads

In order to observe the loads experienced by the aircraft structure, strain gauges are placed on the wings and also at the tail. All the strain gauges are installed in a full Wheatstone bridge configuration to maximise the output sensitivity and reduce the influence of temperature effects. For bending the EA-06-250PD-350 strain gauge was selected and for shear the CEA-06-250US-350 pattern by Micro-Measurements was selected as shown in Fig. 26 and Fig. 27.

The wings were divided into three sections according to the ailerons and the strain gauges were placed at the beginning of each aileron. At each location on the wing, there is one shear strain bridge on the skin in front of the main spar, one behind the main spar and bending strain gauges on the top and bottom skin to complete the full bridge. At the tail, there is a single full bridge strain gauge while the full bridges for bending are completed by having strain gauges on the top and bottom side and left and right side.

**Fig. 26 Strain gauge for bending [6].****Fig. 27 Strain gauge for shear [6].**

To measure the voltage difference over the Wheatstone bridge, the ADS1115 analog to digital converter is used that also includes an up to 16x programmable gain amplifier which allows to measure voltages in the range of $\pm 0.256V$ with a resolution of $7.8\mu V$. With a strain gauge excitation voltage of $5.0V$ and a gauge factor of 2, this allows to measure strains up to ± 25600 microstrain with a resolution of 0.78 microstrain.

A preliminary strain gauge calibration routine was carried out where a known force was applied to the wingtips and tail and the resulting strains were recorded. This allows to establish an initial relationship between the strain gauge measurements and structural loads and obtain estimates of the maximum loading based on the first flight tests. This information can then be used for a more thorough calibration in the future. In Fig. 28 the strains measured on the right wing are presented for the outer, middle and inner sections when wing tip loads of approximately $\pm 0.5kg$ and $\pm 1.0kg$

were applied.

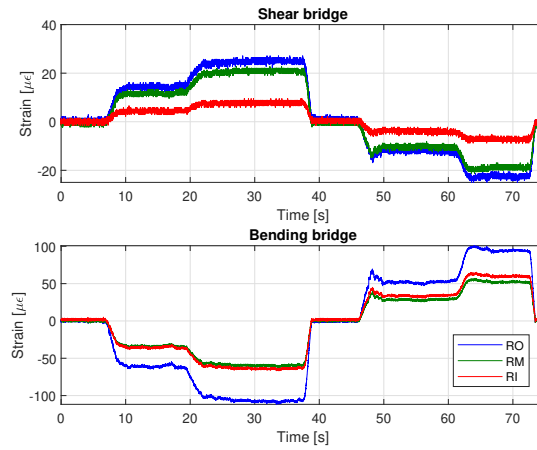


Fig. 28 Right wing strain gauge measurements for known loads.

In addition to the strain gauges, IMUs are also placed inside the wings and the tail in order to complement the strain gauges and capture the acceleration and rotation of the wings and the structure. For this the ICM-20948 IMUs are used which includes a 3-axis accelerometer and 3-axis gyroscope. The sensor also includes a compass but this is currently not used in this setup. The accelerometer is configured to measure up to 8Gs while the gyro is configured to measure rotational rates up to 250 degrees per second.

G. Sensor placement

Using the structural model obtained from the ground vibration testing, it was then possible to evaluate different sensor placement configurations and determine a suitable layout for capturing the structural responses. Automated sensor selection in FEMtools was used to carry out the evaluation. The benefit of using IMUs instead of only accelerometers is the ability to measure the rotational rate at a location without the need to use accelerometers in sets of two. This allowed placing the IMUs in a single line along the wings.

In Fig. 29 an overview of the final integrated sensor positions is presented. Sensor positions on both wings are symmetric while here the strain gauge locations are presented on the right wing and IMUs on the left wing for clarity. At each strain gauge location there are three full bridge strain gauges as described before.

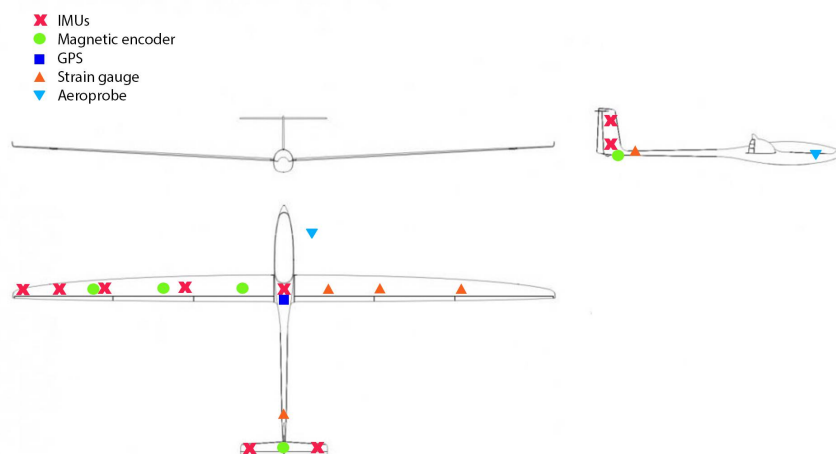


Fig. 29 Diana 2 sensor placement overview.

H. Data acquisition system performance overview

As described before, the data acquisition system consist of Teensy 4 development boards that collect the measurements from individual sensors and a Raspberry Pi 4 which receives the data from all the boards and stores it. The individual sensors do not have a common trigger signal to start the measurements but instead each Teensy board has its own continuous loop where each sensor measurements are triggered, then read and sent to the Raspberry Pi. As the number and type of sensors connected to each Teensy is different, so are the specific sampling rates that were achieved for each sensor. In Table 7 an overview of the average sampling rates achieved by the DAQ are presented for each type of sensor to give an indication of the data acquisition system performance.

Table 7 Overview of the measured signals.

Signal	Symbol	Sampling rate [Hz]
Aerodynamic parameters	V_t, α, β	200
Aircraft position	x, y, z	14
Aircraft cg acceleration	$A_{cg_{xyz}}$	250
Aircraft cg rotational rate	$\omega_{cg_{xyz}}$	250
Control surface angle	δ_i	50
Control surface angle commands	$\delta_{i_{cmd}}$	45
IMUs	$A_{i_{xyz}}, \omega_{i_{xyz}}$	400
Strain gauges	ϵ_i	200

IV. Conclusion

This work has described the development of an aeroservoelastic flight testing platform for the study of flexible aircraft system identification. As part of this study a 1:3 scaled Diana 2 glider model was acquired. An overview of this platform was given together with the main technical parameters and equipment such as the servos and the main engine. The moment of inertia of the aircraft was then estimated using an experimental swing setup and a ground vibration test was conducted to identify the structural modes and natural frequencies. In order to model the control surface dynamics, the control surface responses to sine sweeps and step inputs were recorded. Furthermore, a low cost and modular data acquisition system was developed and integrated into the aircraft for which a detailed overview of the chosen sensors is given together with the sampling times achieved for the whole system. With the scaled Diana 2 glider operational together with its instrumentation system, it is now possible to start flight testing and collecting measurements for system identification purposes.

References

- [1] Grauer, J. A., and Boucher, M. J., "Real-time parameter estimation for flexible aircraft," *2018 Atmospheric Flight Mechanics Conference*, American Institute of Aeronautics and Astronautics, 2018. <https://doi.org/10.2514/6.2018-3155>.
- [2] de Oliveira Silva, B. G., "System Identification of Flexible Aircraft in Time Domain," Ph.D. thesis, Technical University of Braunschweig, aug 2018.
- [3] Baudismodel.com, "Diana 2 (scale 1/3)," 2021. URL <https://www.baudismodel.com/en/production/k2408-actual-production/3-diana-2-scale-1-3.html>, (accessed: 01.12.2021).
- [4] Kotikalpudi, A., Taylor, B., Moreno, C., Pfifer, H., and Balas, G. J., "Swing Tests for Estimation of Moments of Inertia," Tech. rep., 2013.
- [5] Genta, G., and Delprete, C., "Some considerations on the experimental determination of moments of inertia," *Meccanica*, Vol. 29, No. 2, jun 1994, pp. 125–141. <https://doi.org/10.1007/BF01007497>.
- [6] Micro-Measurements, "Precision Strain Gages and Sensors," , Feb 2016. URL <http://www.vishaypg.com/docs/50003/precsg.pdf>.